REPORT DOCUMENTATION PAGE

Form Approved OMB No. 0704-0188

1. REPORT DATE *(DD-MM-YYYY)*	2. REPORT TYPE	3. DATES COVERED *(From – To)*
07-05-2010	Final Report	12 March 2009 - 12-Mar-10

4. TITLE AND SUBTITLE

Increased Order Modeling Approach to Unsteady Aerodynamics and Aeroelasticity

5a. CONTRACT NUMBER
FA8655-09-1-3062

5b. GRANT NUMBER

5c. PROGRAM ELEMENT NUMBER

6. AUTHOR(S)

Professor Moti Karpel

5d. PROJECT NUMBER

5d. TASK NUMBER

5e. WORK UNIT NUMBER

7. PERFORMING ORGANIZATION NAME(S) AND ADDRESS(ES)

Technion - Istael Institute of Technology
Haifa 32000
Israel

8. PERFORMING ORGANIZATION REPORT NUMBER

N/A

9. SPONSORING/MONITORING AGENCY NAME(S) AND ADDRESS(ES)

EOARD
Unit 4515 BOX 14
APO AE 09421

10. SPONSOR/MONITOR'S ACRONYM(S)

11. SPONSOR/MONITOR'S REPORT NUMBER(S)
Grant 09-3062

12. DISTRIBUTION/AVAILABILITY STATEMENT

Approved for public release; distribution is unlimited.

13. SUPPLEMENTARY NOTES

14. ABSTRACT

Increased-Order Modeling (IOM) is a practical and efficient approach to the modeling of dynamic systems that are mostly linear, but their behavior may be significantly affected by local nonlinearities. The approach is based on the augmentation of a main linear block with nonlinear feedback loops that represent the important system nonlinearities. The report outlines a new IOM-based framework for nonlinear aeroelastic simulations. Previously conducted aeroelastic studies with nonlinear structural and control elements are presented in a unified and systematic manner within the new framework, and new studies with nonlinear unsteady aerodynamics are initialized.

The framework is based on two recently developed schemes for dynamic loads on linear aeroelastic systems with control systems that include significant nonlinear elements such as displacement limits and activation zones. The solution sequence starts in the first scheme with the calculation of frequency response functions of the linear aeroelastic system. The modal response is then calculated using Fast-Fourier-Transform (FFT) techniques with the nonlinear elements replaced by linear ones. The response is then corrected by incremental nonlinear effects in a process that combines time domain solutions of the nonlinear elements and convolution integrals for the linear parts with impulse response functions based on the frequency-domain plant model. The second scheme is based on time-domain models that use rational-function approximation of the unsteady aerodynamic force coefficients to generate state-space aeroservoelastic equations of motion of the linear plant. The model has been expanded to accommodate nonlinear control elements by using common utility software packages such as Matlab/Simulink.

The computational processes with nonlinear control were generalized to accommodate local structural and aerodynamic nonlinearities as well, under the IOM framework. Five different nonlinear aeroelastic problems are posed and solved in the IOM framework. The cases are dynamic response to gusts with nonlinear control, dynamic simulation of a maneuvering air vehicle with actuator free play, limit-cycle oscillations (LCO) of platetype fins with nonlinear plate-stiffness components, wing-store LCO with nonlinear aerodynamics, and dynamic gust loads with nonlinear aerodynamics. These proof-of-concept applications demonstrate the potential, practicality and wide usage of the IOM approach.

15. SUBJECT TERMS
EOARD, Unsteady Aerodynamics, Flutter Suppression, Aeroelasticity

16. SECURITY CLASSIFICATION OF:			17. LIMITATION OF ABSTRACT	18, NUMBER OF PAGES	19a. NAME OF RESPONSIBLE PERSON
a. REPORT	b. ABSTRACT	c. THIS PAGE			Surya Surampudi
UNCLAS	UNCLAS	UNCLAS	UL	36	19b. TELEPHONE NUMBER *(Include area code)* +44 (0)1895 616021

Final report on EOARD Award FA8655-09-1-3062

Increased Order Modeling Approach to Unsteady Aerodynamics and Aeroelasticity

Moti Karpel

Technion – Israel Institute of technology,

Haifa, Israel

March 2010

Table of Contents

Summary

Increased-Order Modeling (IOM) is a practical and efficient approach to the modeling of dynamic systems that are mostly linear, but their behavior may be significantly affected by local nonlinearities. The approach is based on the augmentation of a main linear block with nonlinear feedback loops that represent the important system nonlinearities. The report outlines a new IOM-based framework for nonlinear aeroelastic simulations. Previously conducted aeroelastic studies with nonlinear structural and control elements are presented in a unified and systematic manner within the new framework, and new studies with nonlinear unsteady aerodynamics are initialized.

The framework is based on two recently developed schemes for dynamic loads on linear aeroelastic systems with control systems that include significant nonlinear elements such as displacement limits and activation zones. The solution sequence starts in the first scheme with the calculation of frequency response functions of the linear aeroelastic system. The modal response is then calculated using Fast-Fourier-Transform (FFT) techniques with the nonlinear elements replaced by linear ones. The response is then corrected by incremental nonlinear effects in a process that combines time domain solutions of the nonlinear elements and convolution integrals for the linear parts with impulse response functions based on the frequency-domain plant model. The second scheme is based on time-domain models that use rational-function approximation of the unsteady aerodynamic force coefficients to generate state-space aeroservoelastic equations of motion of the linear plant. The model has been expanded to accommodate nonlinear control elements by using common utility software packages such as Matlab/Simulink.

The computational processes with nonlinear control were generalized to accommodate local structural and aerodynamic nonlinearities as well, under the IOM framework. Five different nonlinear aeroelastic problems are posed and solved in the IOM framework. The cases are dynamic response to gusts with nonlinear control, dynamic simulation of a maneuvering air vehicle with actuator free play, limit-cycle oscillations (LCO) of plate-type fins with nonlinear plate-stiffness components, wing-store LCO with nonlinear aerodynamics, and dynamic gust loads with nonlinear aerodynamics. These proof-of-concept applications demonstrate the potential, practicality and wide usage of the IOM approach.

1 Introduction

Extensive research has been conducted in recent years on reduced-order modeling (ROM) of aeroelastic systems that starts with high-fidelity nonlinear computational schemes. The IOM approach investigated in this project attempts to model nonlinear aeroelastic systems in a different way. It is based on linear models that are supplemented with nonlinear feedback loop that simulate local nonlinearities identified from high-fidelity models or tests. Generally, the addition of nonlinear elements to linear models has been used by engineers, one way or another, when dealing with nonlinear systems. The current project aims at developing a systematic IOM framework that exploits as much as possible the numerical advantages in dealing with linear systems while keeping the complexity of the added nonlinear elements as low as required for obtaining adequate accuracy in aeroelastic applications.

The basic IOM methodology has already been applied to aeroelastic models with nonlinear control elements [1, 2] and to local structural nonlinearities, such as to actuator free play [3] and to nonlinear plates [4], and gave excellent predictions of limit-cycle oscillations (LCO) compared to fully non-linear solutions and wind-tunnel tests. Preliminary attempts to predict aerodynamically-induced LCO of wing-store fighter configurations using IOM, Ref. 5, showed promising trends but did not reach adequate accuracy yet. These attempts are resumed in the current project as detailed later in this report.

The linear parts in Refs. 2 to 5 were based on generalized-coordinate state-space equations of motion of the aeroelastic plants, and the nonlinearities are expressed as feedback loops as shown in the scheme of Figure 1. The state-space models were constructed in these applications with unsteady aerodynamics panel models of the ZAERO code using the Minimum-State rational function approximation technique of Ref. 6. The feedback signals in the free-play investigation of Ref. 3 are the relative rotations between the two ends of the actuators. The feedback is based on the actuator forces that are zero when the rotation is in the free-play zone. The feedback signals in the wing-store LCO model of Ref. 5 are the lift and moment coefficients in wing strips along the wing span. The feedback is based on CFD-generated information regarding aerodynamic loads when the wing vibrates, as explained and expanded in the following sections.

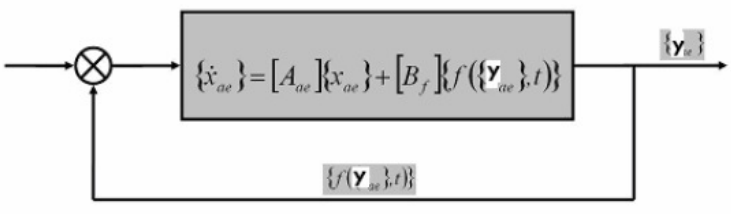

Figure 1: General scheme of state-space based IOM

The IOM approach was applied in Ref. 1 to dynamic gust loads with nonlinear control systems. Since the state-space model of the linear aeroelastic system might be insufficiently robust in industrial applications, the response was based on frequency-domain model of the aeroelastic plant and convolution integrals that introduce the nonlinearity of the control elements. FFT techniques that are used for calculating the linear response and the impulse responses for the convolution process lead to a very efficient and robust loads calculation process. The same modeling approach is being used in the current research for calculating dynamic response to gust loads with nonlinear aerodynamics, as detailed below, based on CFD response data generated by EZNSS code using the the techniques of Refs. 10 to 12.

2 Methods, Assumptions and Procedures

2.1 The IOM Approach

The IOM approach is based on the assumption that the results of an analysis with a linear model can serve as a good starting point for the nonlinear investigation. The general steps are as following:

1. Start with a linear aeroelastic model.
2. Identify nonlinear effects that might affect the results significantly .
3. Add nonlinear corrections that adequately represent key nonlinear effects.
4. Formulate the problem based on a main linear block and nonlinear feedback loops.
5. Perform simulations in a way that takes advantage of the IOM formulation.
6. Verify/update the models by comparisons with selected tests and/or high-fidelity solutions of rigid and elastic vehicles.

Previous research efforts at Technion established two “plug-and-play” software packages for various IOM applications:

- Matlab/Simulink code with time-domain models where the main linear block is based on state-space models imported from the ZAERO software package.
- The DYNRESP code where the main linear block uses frequency-domain models to provide the baseline response, and nonlinear feedback loops to modify the response using convolution integrals.

The application procedure of the IOM approach to various nonlinear aeroelastic problems is detailed in the following subsections. Results are given and discussed in Chapter 3.

2.2 Response to dicrete gust excitation with nonlinear control

The process developed in Ref. 1 for gust-response simulations with nonlinear control is generalized in this work as a framework for the various IOM applications described below. A typical block diagram of the IOM process with nonlinear control is shown in Figure 2. The system is divided into 3 blocks. The main linear block includes the linear aeroelastic system, the actuators, sensors and directly-connected linear control elements. The nonlinear block includes the nonlinear control elements and the isolated-linear block includes linear control elements that are embedded inside the nonlinear block. The assembled nonlinear and isolated linear block is called below the NLIL block.

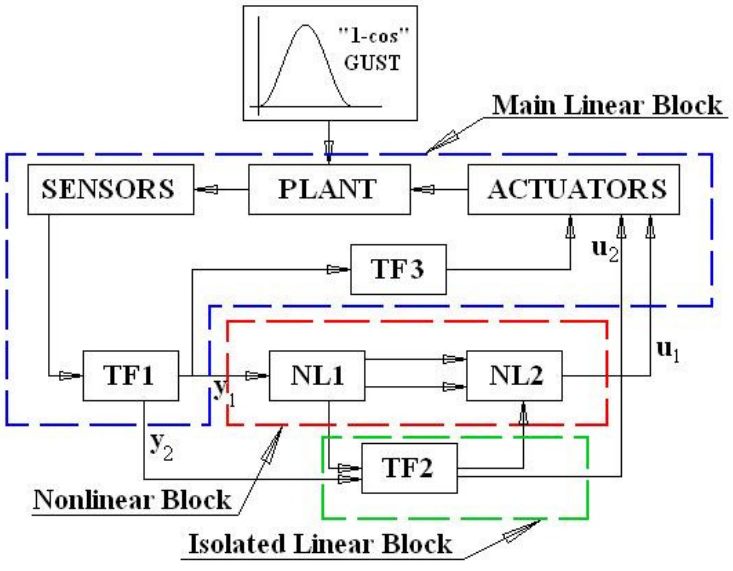

Figure 2: Blocks of IOM for gust response with nonlinear control

The computation process is based on 3 stages:

- Stage 1: Frequency-domain (FD) response of the main linear block to gusts and control commands u_i with the nonlinear block disconnected.
- Stage 2: Generation of time-domain (TD) response signals of the linear block to the gust and to unit u_i impulses using FFT/IFFT techniques.
- Stage 3: Addition of nonlinear effects based on nonlinear models and convolution with impulse responses.

The solution sequence starts with FD linear response of the vehicle to gust excitation with the NLIL block disconnected:

$$\left\{x_{vG_L}(i\omega)\right\} = \left[\bar{A}_v(i\omega)\right]^{-1}\left\{B_{vw}(i\omega)\right\}\frac{w_G(i\omega)}{V} \tag{1}$$

where $\left\{x_{vG_L}(i\omega)\right\}$ is the vector of modal displacements and linear control states, $\left[\bar{A}_v(i\omega)\right]$ is the system dynamic matrix, $w_G(i\omega)$ is the gust velocity amplitude and V is the vehicle velocity. The same $\left[\bar{A}_v(i\omega)\right]^{-1}$ is efficiently used for calculating the FD linear response vectors to actuator impulses:

$$\left[X_{vU}(i\omega)\right] = \left[\bar{A}_v(i\omega)\right]^{-1}\left[\bar{B}_v\right] \tag{2}$$

which will be used later for adding the effects of the nonlinear and isolated linear blocks based on the linear sensor response vectors associated with Eqs. (1) and (2),

$$\left\{y_L(i\omega)\right\} = \left[C_v(i\omega)\right]\left\{x_{vG_L}(i\omega)\right\} \tag{3}$$

and

$$\left[Y_{LU}(i\omega)\right] = \left[C_v(i\omega)\right]\left[X_{vU}(i\omega)\right] \tag{4}$$

FFT of the FD vectors of Eqs. (3) and (4) yield the TD response vectors $\left\{y_L(t)\right\}$ and $\left[Y_{LU}(t)\right]$. The nonlinear solution progresses in time from this point where in each step the sensor response to the previous-step input from the NLIL block is calculated by the convolution integral

$$\left\{y(t)\right\} = \left\{y_L(t)\right\} + \int_0^{t_{con}} \left[y_{LU}(t-\tau)\right]\left\{u(\tau)\right\}d\tau \tag{5}$$

From which the progressive nonlinear feedback $\left\{u(t)\right\}$ is calculated according to the nonlinear and isolated-linear blocks.

2.3 Response to maneuver command with actuator free play

A common strong nonlinearity which may affect the aeroelastic vibration level and the response to actuator commands is free play in the actuator connections to the control surfaces. We consider here a flight vehicle with two ailerons, one on each wing. The free plays in the two actuators are assumed to be the only nonlinearity in the system. The right and left ailerons are entering, in their turns, into their free-play zones while the vehicle is maneuvering in response to roll commands.

A block diagram of the IOM system is depicted in Figure 3. A detailed description of the formulation and the numerical application is given in Ref. 3. The plant is represented by time-domain state-space equations of motion based on structural normal modes with floating ailerons, which serve as generalized coordinates, and rational function approximation of the associated generalized unsteady aerodynamic force coefficient matrices. Structural elements that connect the actuator outputs to the control surfaces are considered in the linear-feedback FORCES box. The differences y_1 and y_2 between the actuator rotation commands, δ_{cR} and δ_{cL}, and the respective actual control surface rotations, δ_R and δ_L, and multiplied by the stiffness of the connection elements to produce the driving forces. With the nonlinear block disengaged, the main linear block produces the linear response of the vehicle to the maneuver commands.

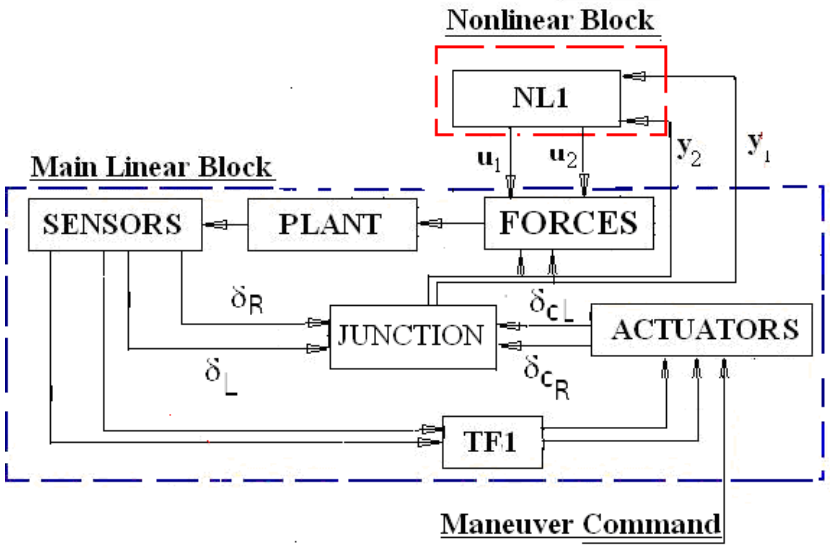

Figure 3: Blocks of IOM for maneuver simulation with actuator free play

When the nonlinear block is engaged, the FORCES box operates on the sums of y_i and u_i. The outputs y_1 and y_2 are read by the nonlinear element NL1 that produces the u_1 and u_2 inputs to the linear block in Figure 3. When y_i is inside the respective free-play zone between δ_F and $-\delta_F$, the respective output of NL1 is $u_i=-y_i$ such that the resulting actuation force becomes zero. When y_i is out of the free-play zone, $u_i=\delta_F$ or $-\delta_F$ to produce the aileron displacement shift caused by the free play.

In addition to the application of the IOM modeling approach, Ref. 3 presented and discussed three other interesting modeling aspects that are different than the standard aeroservoelastic modeling procedures. These are the application of direct actuation forces without defining separate control-surface deflection modes, the use of fictitious masses at the control-surface rotation degrees of freedom, and the account for asymmetry caused by asymmetric activation of the control surfaces.

The direct-force modeling is necessary because the control-mode modeling approach of Ref. 6 collapses when the actuator stiffness becomes zero. The fictitious masses are needed to allow a full representation of the local actuator deformations in the modal-based formulation. The structural rotation degrees of freedom, y_1 and y_2 are loaded in the normal-modes analysis by large fictitious inertial terms. There inertias are later subtracted during the simulation process. The asymmetric motion is facilitated by using both symmetric and anti-symmetric modes, generated separately, in the model. The coupling between them is caused by the nonlinear block.

2.4 Flutter of solid fins with nonlinear plate elements

Solid aerodynamic fins are often made of machined solid materials. Wind-tunnel investigations of such fins demonstrated limit-cycle oscillations (LCO) of amplitudes larger than the average fin thickness. The fin of Ref. 7 was tested in the wind tunnel and analyzed using high-fidelity structural and aerodynamic models. The structure is made of a uniform 9 *mm* steel plate. The fin structural model is shown in Figure 4. Reference 4 used the IOM framework to identify the important nonlinear effect and performed LCO response calculations. Key points, with emphasis on the IOM features are shown below.

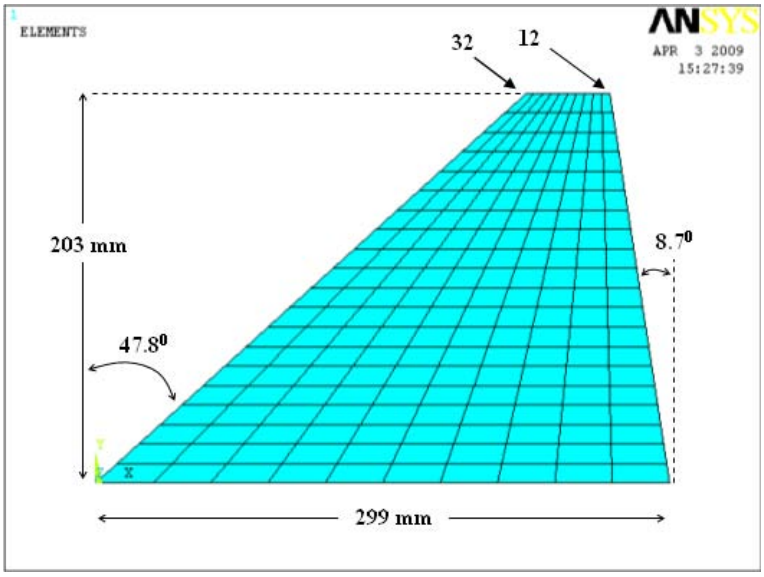

Figure 4: Structural model of the cropped delta wing

The nonlinearity considered in our work is the first nonlinear term in Taylor series of von-Karman's strain equation for plate:

$$\varepsilon = \begin{Bmatrix} \dfrac{\partial u}{\partial x} \\ \dfrac{\partial v}{\partial y} \\ \dfrac{\partial u}{\partial y} + \dfrac{\partial v}{\partial x} \\ -\dfrac{\partial^2 w}{\partial x^2} \\ -\dfrac{\partial^2 w}{\partial y^2} \\ 2\dfrac{\partial^2 w}{\partial x \partial y} \end{Bmatrix} + \begin{Bmatrix} \dfrac{1}{2}\left(\dfrac{\partial w}{\partial x}\right)^2 \\ \dfrac{1}{2}\left(\dfrac{\partial w}{\partial y}\right)^2 \\ \left(\dfrac{\partial w}{\partial x}\right)\left(\dfrac{\partial w}{\partial y}\right) \\ 0 \\ 0 \\ 0 \end{Bmatrix} = \begin{Bmatrix} \varepsilon^{pl} \\ \varepsilon^{b} \end{Bmatrix} = \begin{Bmatrix} \varepsilon_0^{pl} \\ \varepsilon_0^{b} \end{Bmatrix} + \begin{Bmatrix} \varepsilon_{NL}^{pl} \\ 0 \end{Bmatrix} \tag{6}$$

A time-domain state-space aeroelastic model for the clamped fin with linear plates and excitation forces is

$$\begin{Bmatrix} \dot{\xi} \\ \ddot{\xi} \\ \dot{x}_a \end{Bmatrix} = \begin{bmatrix} 0 & I & 0 \\ -\left[\bar{M}\right]^{-1}\left[K + qA_0\right] & -\left[\bar{M}\right]^{-1}\left[C + \frac{qL}{V}A_1\right] & -q\left[\bar{M}\right]^{-1}\left[D\right] \\ 0 & \left[E\right] & \frac{V}{L}\left[R\right] \end{bmatrix} \begin{Bmatrix} \xi \\ \dot{\xi} \\ x_a \end{Bmatrix} + \begin{Bmatrix} 0 \\ \left[\bar{M}\right]^{-1} \\ 0 \end{Bmatrix} \{F\} \tag{7}$$

where $\left[\bar{M}\right] = \left[M\right] + \frac{qL^2}{V^2}\left[A_2\right]$ and use is made of the generalized mass, damping and stiffness matrices, [*M*], [*C*] and [*K*], of the structural model with linear plates and the coefficient matrices of the minimum-state rational-function approximation of the unsteady aerodynamics [6]

$$\left[Q(s)\right] = \left[A_0\right] + \frac{L}{V}\left[A_1\right]s + \frac{L^2}{V^2}\left[A_2\right]s^2 + \left[D\right]\left(\left[I\right]s - \frac{V}{L}\left[R\right]\right)^{-1}\left[E\right]s \tag{8}$$

The generalized force vector {*F*} in Eq. (7) may include external forces and nonlinear feedback,

$$\{F\} = -\left[\Delta K(\xi)\right]\{\xi\} + \{F_{ext}\} \tag{9}$$

where [Δ*K*] represents the nonlinear generalized stiffness term associated with the nonlinear term of Eq. (6), as described below.

The IOM block diagram that reflects Eqs. (6)-(9) is shown in Figure 5. The PLANT box contains the linear part of Eq. (7). The DISPLACSEMENTS box converts the modal response {ξ(t)} into discrete displacements at the finite-element degrees of freedom. The co-rotational approach is used in the nonlinear block to separate the rigid-body and elastic deformations of each element [4] and the elastic deformations are used for calculating the added nonlinear elastic forces. These are converted to generalized coordinates and expressed as [Δ*K*] in the ADDED ELASTIC FORCES block. The resulting {*F*} of Eq. (9) is fed back to Eq. (7) in a time-marching process.

The accuracy of the nonlinear feedback forces was first checked in [4] by solving the static version of Eqs. (7) and (9) with no aerodynamics,

$$\left[K + \Delta K(\xi)\right]\{\xi\} = \{F_{ext}\} \tag{10}$$

where $\{F_{ext}\}$ is a vector of generalized forces based on a constant vertical force at point 32 of Figure 4 and zero elsewhere. An iterative solution of Eq. (10) for $\{\xi\}$, followed by the recovery of the vertical displacement at point 12, yielded the deflection curves of Figure 6 were the 20-mode nonlinear-controller solution and the respective linear solution are compared with full direct solutions by Ansis. It can be observed that the linear solutions are practically identical and that the differences between the nonlinear solutions are small.

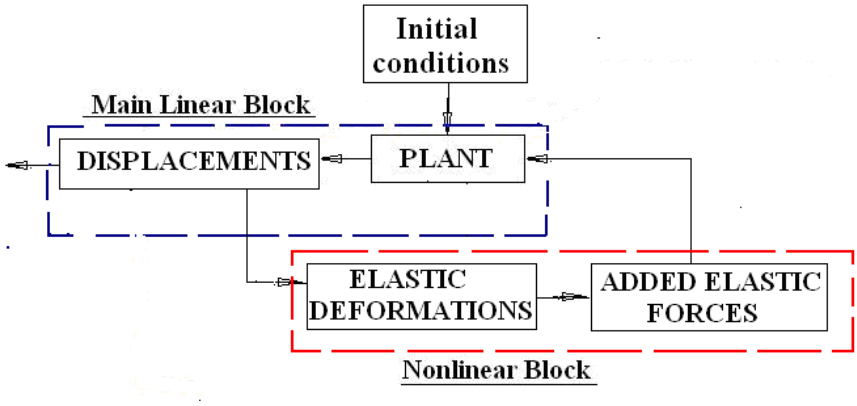

Figure 5: Block diagram of IOM for aeroelastic response of plate-like fin

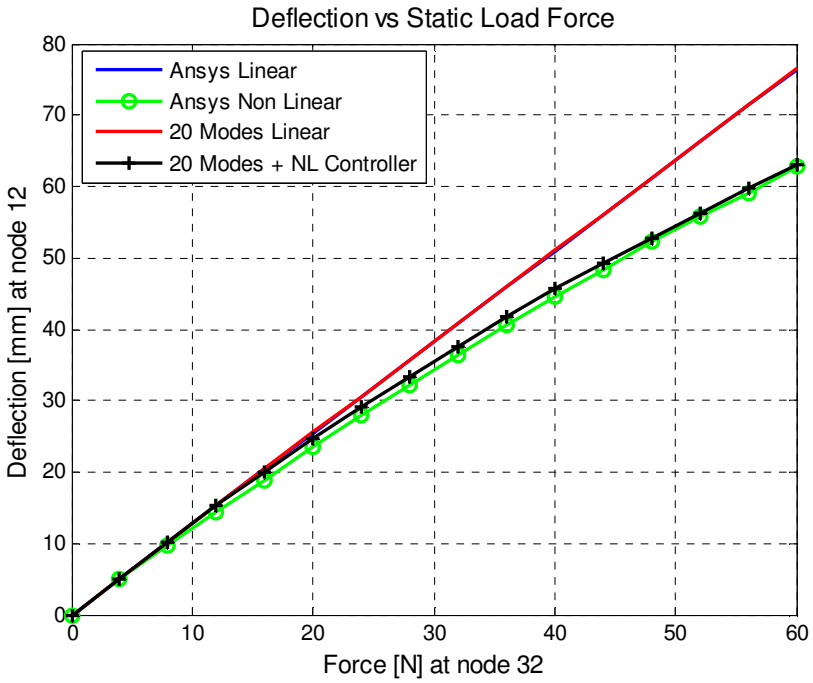

Figure 6: Static displacement curves of the cropped wing

2.5 Wing-Store LCO

The IOM block diagram for aeroelastic response to initial conditions with nonlinear aerodynamics is depicted in Figure 7. The PLANT is based on the linear state-space model of Eq. (7) above (without the excitation term), based on the rational aerodynamic approximation of Eq. (8). The response is obtained by numerical integration starting from user defined initial conditions. The load-mode option of ZAERO can be used for expressing the linear local lift and moment coefficients at strips along the wing span as functions of the modal state response. These coefficients define the would-be aerodynamic loads, if the system was linear, in the AERODYNAMIC FORCES box of Figure 7. The AERODYNAMIC CORRECTIONS box of the nonlinear block compares these forces with the local nonlinear force models and introduce the nonlinear correction feedback.

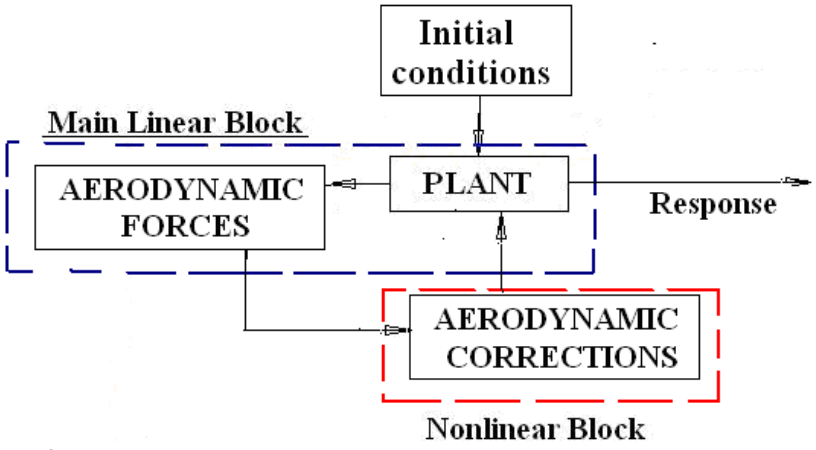

Figure 7: IOM blocks for aeroelastic response with nonlinear aerodynamics

The application of the IOM approach to the construction of aeroelastic models for LCO simulations with nonlinear unsteady aerodynamics is based on the following steps:

1. Identification of a store configuration that might cause LCO in the flight envelope.
2. Linear flutter analysis and parametric studies to identify a baseline flutter mechanism to which the LCO is related.
3. Rational function approximations of the generalized aerodynamic matrices and the associated lift and moment coefficients at the wing strips.
4. Generation of a linear state-space time-domain model that predicts the linear flutter and includes the lift and moment coefficients of the wing strips as output parameters.
5. Definition of a baseline nonlinear behavior based on steady CFD solutions vs. angles of attack (AOA) within the range of the anticipated LCO.
6. Generation of baseline feedback loops that introduce local nonlinear inputs in a way that produces LCO, and their augmentation to the linear state-space model to create the baseline IOM model.

7. IOM time simulations at post-flutter conditions and extraction of structural response histories during LCO.
8. High-fidelity computations with the LCO mode and amplitude as prescribed motion, and comparisons with the IOM simulations.
9. Identification of dynamic nonlinear feedback loops in the state-space models that improve the agreement with high-fidelity results.
10. Iterations between the IOM and the CFD models until satisfactory agreements of monitoring parameters are obtained.
11. Approval by comparisons with high-fidelity computational aeroelasticity results and by satisfying the equilibrium equations.

Satisfactory results in applications to typical cases may lead to a practical design model for a family of LCO cases, such as wing-store LCO, which is computationally efficient and is based on physical insight to the main LCO parameters.

2.6 Dynamic gust loads with nonlinear aerodynamics

The IOM approach to the construction of aeroelastic models for gust-response simulations with nonlinear unsteady aerodynamics is similar to that depicted in Figure 7, but with the initial-condition block replaced by a gust excitation block as in Figure 2. As in the wing-store LCO case of the previous subsection, the IOM process is performed by the application of nonlinear direct-force feedback that is tuned to reflect static and dynamic nonlinear characteristics of the aerodynamic loads due to the encounter of discrete gusts, as detailed in Section 3.5 below.

Unlike in the LCO investigation of the previous section, The gust-response IOM used frequency-domain formulation for calculating the response of the main linear block before the nonlinear feedback forces are added, as done in Section 2.2 above. The AERODYNAMIC FORCES box of Figure 7 calculates the frequency-domain would-be aerodynamic forces at the panel centers by

$$\left\{L_j\left(i\omega\right)\right\} = q\left[A_{jh}\left(i\omega\right)\right]\left\{\xi\left(i\omega\right)\right\} \tag{11}$$

where $\left[A_{jh}\left(i\omega\right)\right]$ is interpolated from the unsteady [AJH(ik)] matrices exported from ZAERO. These loads are transformed to the time using IFFT before being used at inputs to the nonlinear feedback loops.

3 Results and Discussions

3.1 Gust loads on Generic Transport Aircraft with nonlinear control

Gust response parameters of the Generic Transport Aircraft (GTA) of Ref. 1 are presented here to demonstrate the IOM application with nonlinear control system presented in section 2.2 above. The structural and aerodynamic models are shown in Figure 8. Eleven symmetric modes up to 45 Hz are used. The control system consists of symmetrically activated ailerons and is based on measuring the vertical acceleration near CG. The response to a regulation '1-cos' vertical discrete gust is calculated.

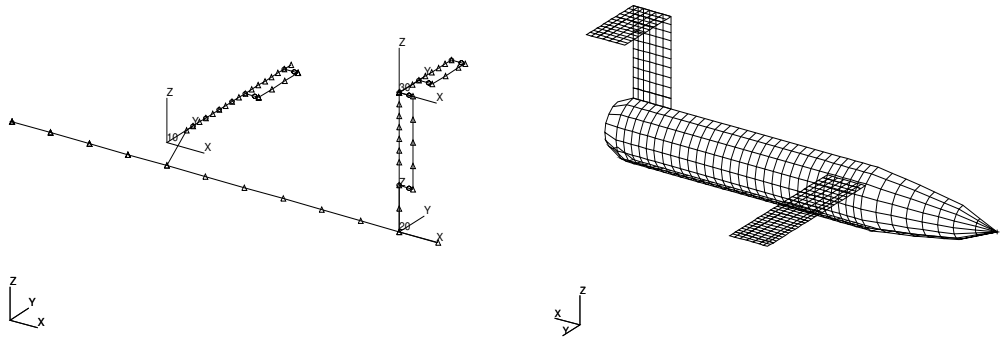

Figure 8: GTA structural and aerodynamic models

A diagram of the flight control system is shown in Figure 9. The main blocks are: TF1: basic linear control law; NL1: Cluster of nonlinear elements whom main features are limiting the deflections and rates, holding peak deflections for 0.5 seconds before starting a gradual decay and a minimal deflection command of 1 degree; TF2: enforcement of slow decay; and NL2: a selection switch.

The responses of two rigid-body and two elastic modes, obtained with FFT-based frequency-domain and time-domain formulations of the main linear block are compared in Figure 10. The differences in the rigid-body responses (Modes 1, 2) are due to the enforced return of the FFT response to zero at the end of the time window of 8.2 seconds, but this difference has negligible effects on the resulting loads, as can be deduced from the practically perfect fit of the elastic-mode responses.

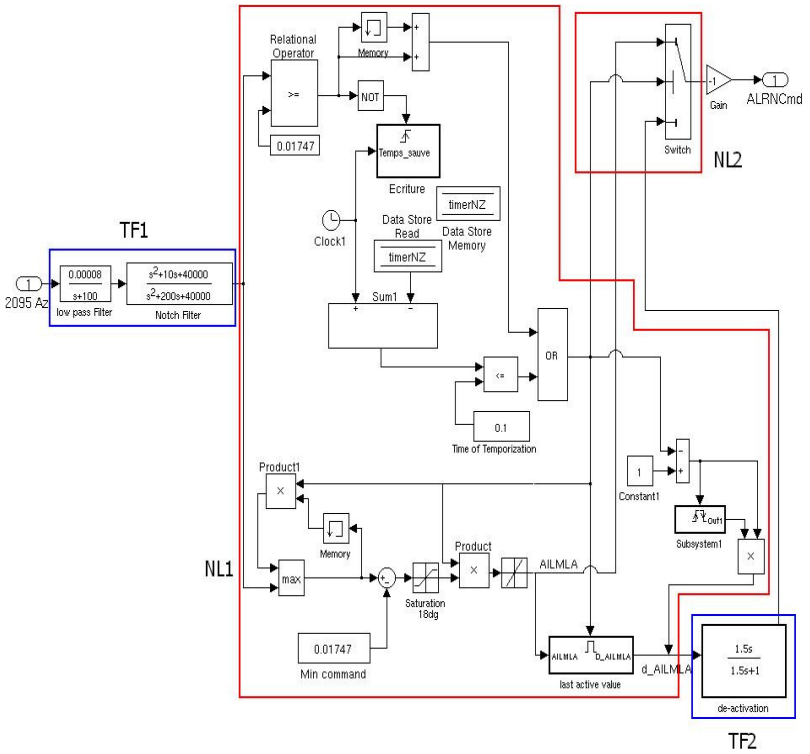

Figure 9: The nonlinear control system in the GTA gust response

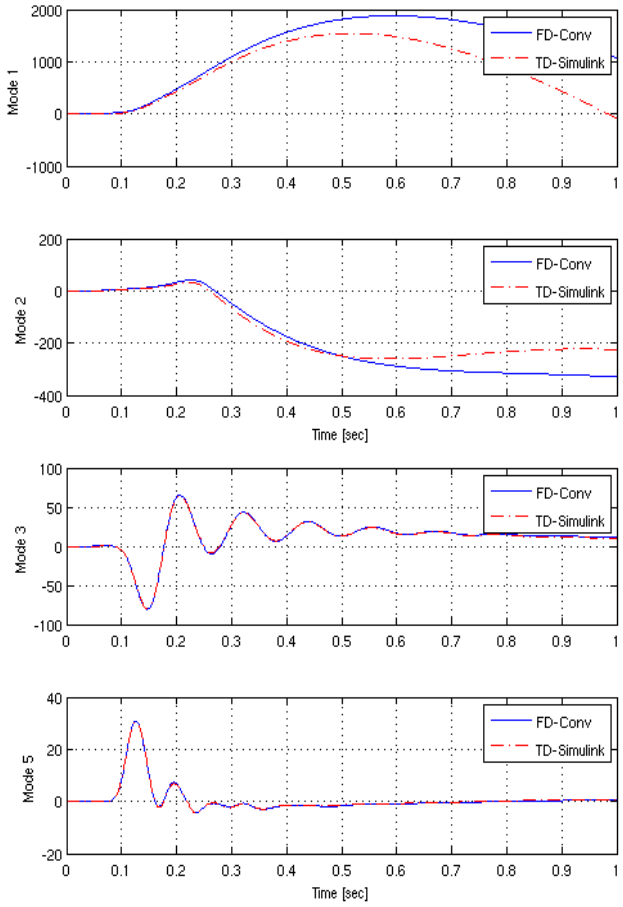

Figure 10: Modal response, 2 rigid-body and 2 elastic modes

The actuator response in the nonlinear case is compared in Figure 11 to that of the linear response, where the output of TF1 is connected directly to the actuator. The time histories of the wing-root bending moment with no control, with linear control and with nonlinear control are compared in Figure 12. It can be observed that the control system alleviates the maximal bending moment significantly.

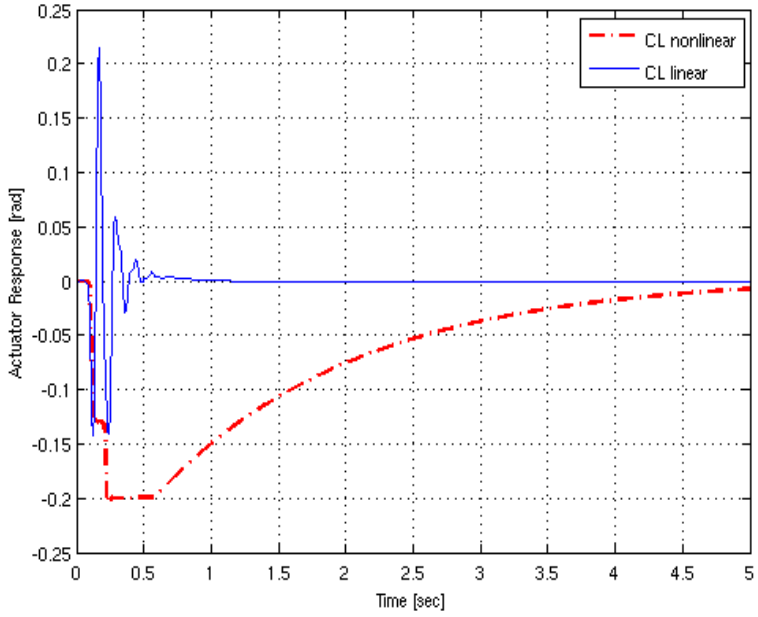

Figure 11: Actuator response, linear and nonlinear FCS

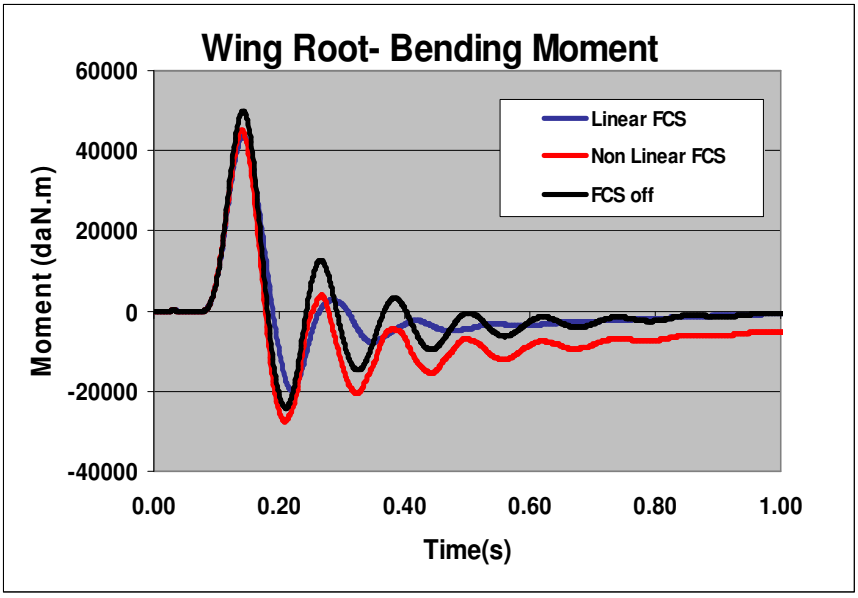

Figure 12: Wing root bending moment of GTA in response to a discrete gust

3.2 LCO Simulations with actuator free play

The structural and aerodynamic models that were used for the numerical example of Ref. 3 are shown in Figure 13. Selected results of are presented here to demonstrate the IOM application to aeroelastic LCO simulation with actuator free play. The plant model in the IOM block diagram of Figure 3 was constructed in a state-space form that included symmetric and anti-symmetric modes extracted from separate finite-element models. The two mode groups are coupled during the simulations when one of the ailerons enters the free-play zone while the other one does not. The full formulation is given in Ref. 3.

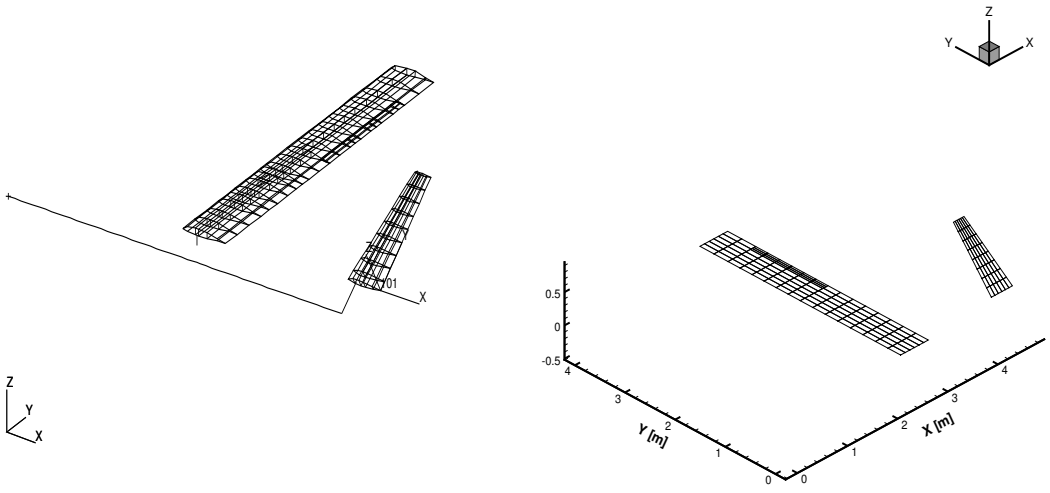

Figure 13: Structural and aerodynamic models of a UAV for free-play analysis

The first simulation is without a control system, namely TF1 of Figure 3 is disconnected. The maneuver command drives the right actuator to a -1^{o} steady position and the left one to a 1^{o} position. Figure 14 shows the response of the two aileron deflections. Due to a symmetric free-play of $\pm 0.5^{o}$ at both actuators, the right aileron develops LCO with amplitude slightly larger than the free-play zone around the 1^{o} position. The left aileron is out of its free play zone, but it still vibrates due to the structural vibrations excited by the right aileron.

The second simulation is with a control law at TF1 that controls the aircraft roll maneuvers. The right and left aileron responses, δ_{ar} and δ_{al}, in a typical roll maneuver scenario are compared in Figure 15 to the respective commanded values δ_{cr} and δ_{cl}. It can be

observed that each aileron starts vibrating when entering, in it turn, the free-play zone. When the maneuver command changes slowly, such as between 5 and 32 seconds, the vibrations are significant. However, when the aileron is driven rapidly through the free-play zone, such as at about 72 seconds, the vibrations do not sustain.

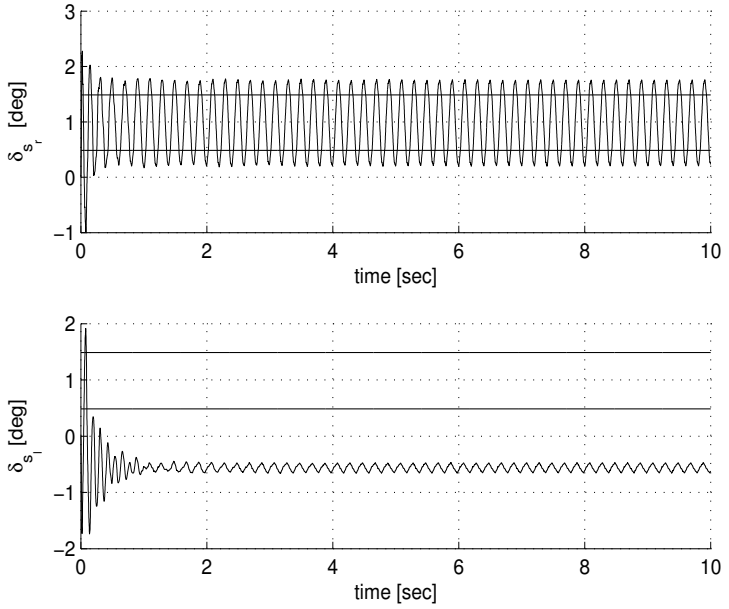

Figure 14: Response of the right and left ailerons to a unit command

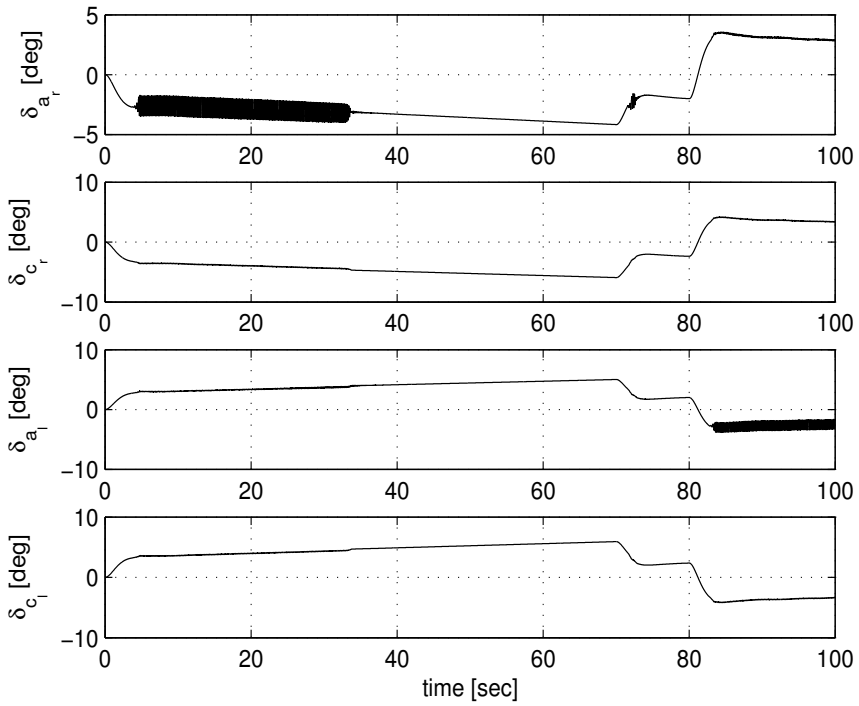

Figure 15: Aileron responses to roll maneuver command.

3.3 Cropped delta wing with plate stiffening

A linear flutter analysis of the cropped delta wing of Section 3.4 and Ref. 4, performed by eigenvalue extractions of the system matrix in Eq. (7), indicated a torsion-bending flutter mechanism at Mach 0.85, q_f=18.96kPa, ω_f=45.6 Hz. The displacement and pitch-angle responses of point 12 to small initial conditions, at several dynamic pressures above q_f, are shown in Figure 16, demonstrating LCO with the amplitudes increase with the dynamic pressure.

The resulting LCO amplitudes and frequencies are compared in Figure 17 with the experimental results and with the computational results of Refs. 7 and 8. Excellent results are shown for the LCO amplitudes up to 23 kPa, and good results are shown for the LCO frequencies. The divergence of the experimental amplitudes at high dynamic pressures may be related to the root cracks that were discovered at the end of the wind tunnel tests. We do not know why the IOM results of [4] are closer to the experiment than the results of Refs. 7 and 8. In any case, it indicates that the main driver of the LCO response is indeed the first von-Karman nonlinearity term, and that the IOM approach is capable of dealing successfully with such nonlinearities.

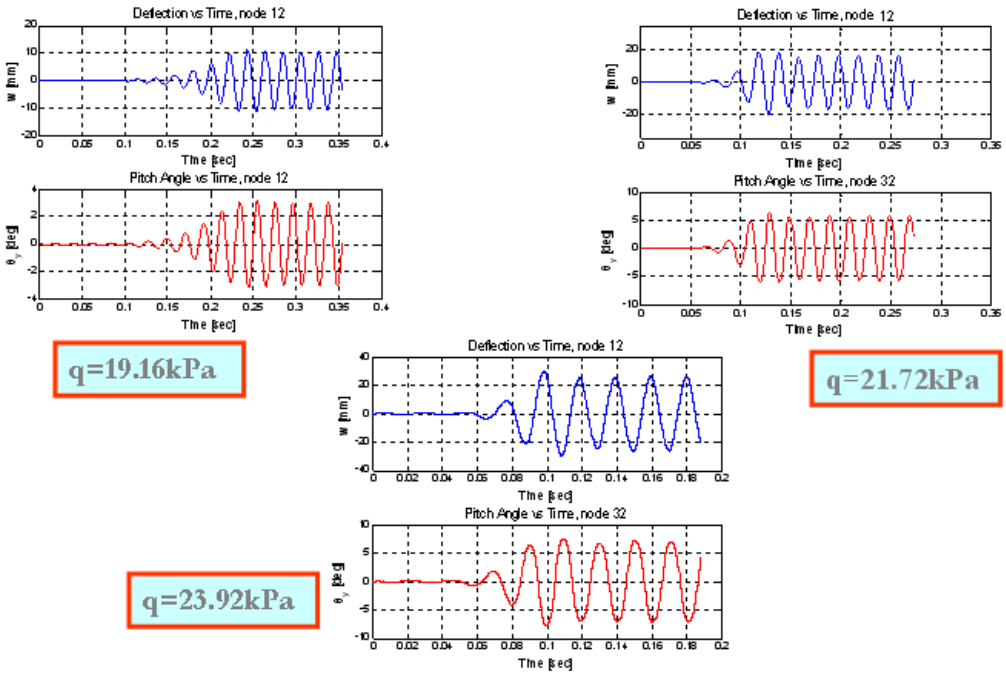

Figure 16: LCO response of the cropped delta wing

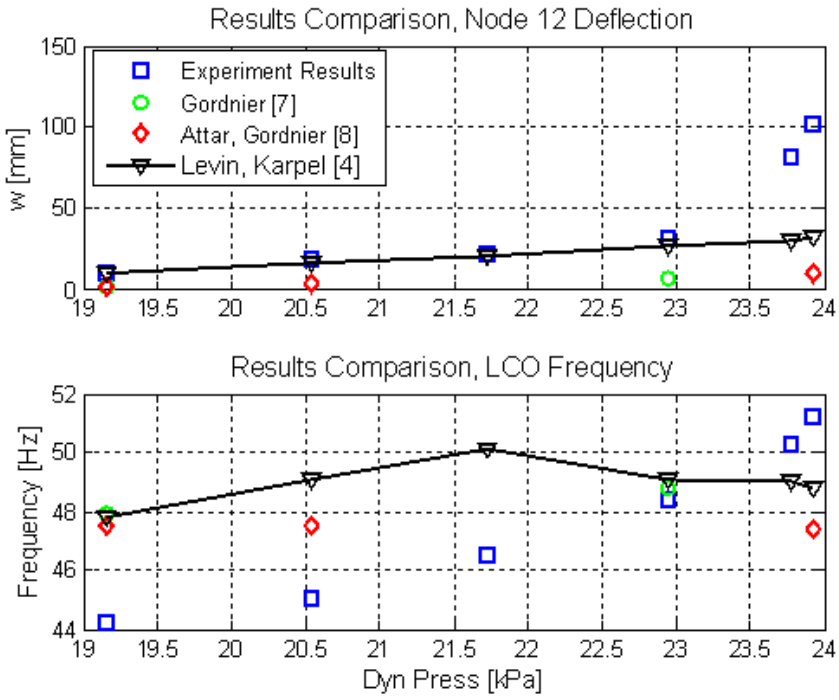

Figure 17: Comparison between LCO test results and numerical solutions

3.4 Wing-store LCO model

3.4.1 Linear flutter analysis with no corrections

The generic advance fighter aircraft (AFA) model used for the numerical applications of this section resembles the F-16 fighter aircraft, but with an about 10% larger wings, with two leading-edge and two trailing-edge wing control surfaces on each wing. Figure 18 shows the structural and the ZAERO aerodynamic panel models of AFA. The symmetric store loading that is used for LCO simulations is detailed in Table 1. The wing-tip missole (1/9) is similar to AIM-9 and the heavy stores are similar to MK-84.

wing station	1/9	2/8	3/7	4/6	CL
store	missile	empty	heavy store	heavy store	---

Table 1: AFA configuration for LCO analyses

The linear aeroelastic model is based on right-side structural NASTRAN model with anti-symmetric boundary conditions. Matched-point linear anti-symmetric flutter analysis in the frequency-domain was carried out at Mach 0.9 using ZAERO. The flutter dynamic

pressure and frequency that were obtained using the g-method are q_F= 2674 *psi*; f_F=6.3 *Hz*. The fact that this dynamic pressure is below sea level is ignored in this investigation. Figure 19 depicts the variations of frequencies and damping coefficients with the dynamic pressure q, exhibiting atypical moderate store flutter mechanism that involves the wing bending and the torsion due to store pitch. Figure 20 depicts some frames of the flutter-mode that reflects coupling between the first two elastic modes, wing bending and tip-missile pitch that causes wing torsion. One can deduce that the outer-wing and the tip-missile aerodynamics play important roles in the flutter mechanism.

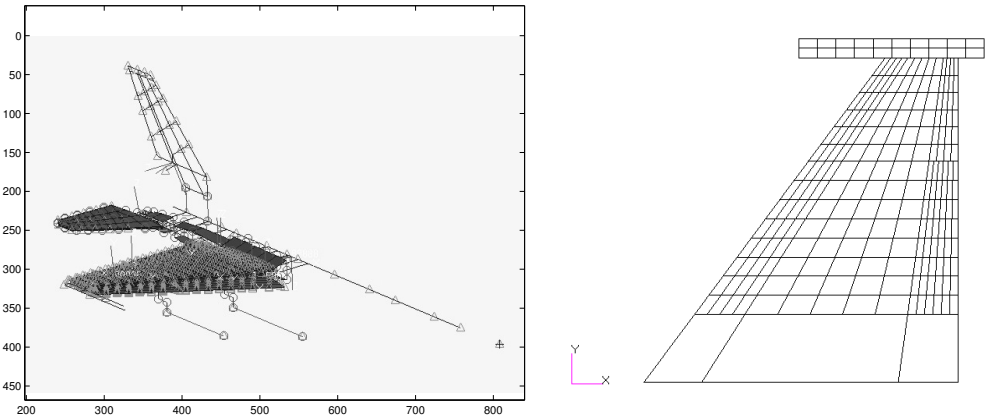

Figure 18 : AFA structural and aerodynamic panel modeling.

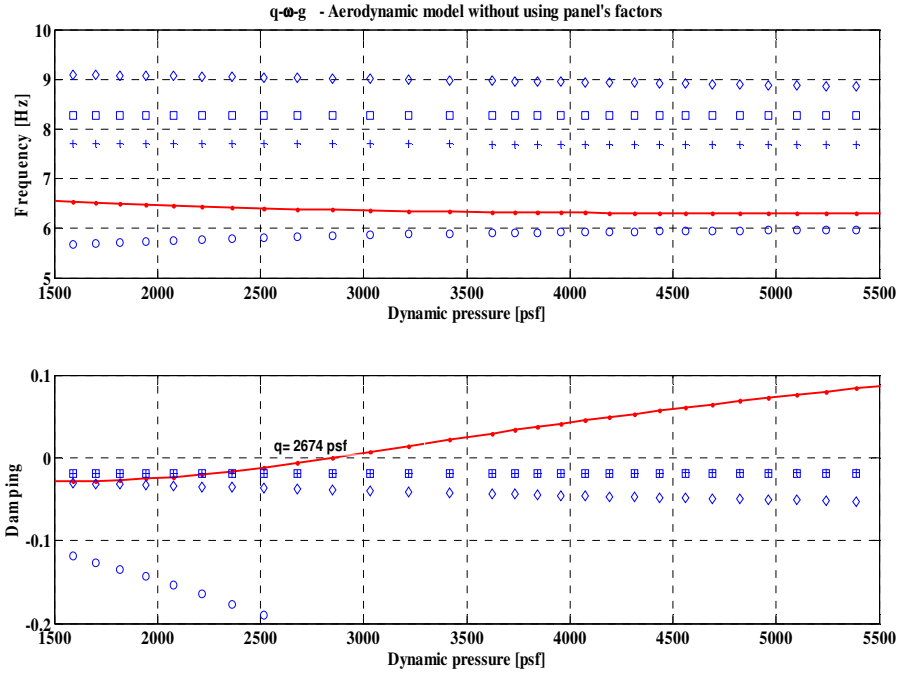

Figure 19: Frequency and damping variations with true air speed

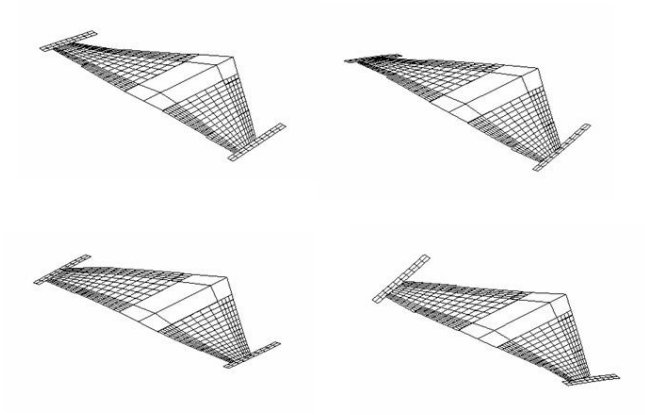

Figure 20: Four frames of the flutter-mode

3.4.2 Nonlinear (CFD) and linear (ZAERO) static solutions

The CFD results presented in this subsection were generated in cooperation with the Israeli CFD Center and the Israeli Air Force in a numerical investigation of LCO. In order to assess to nonlinear nature of the flow field about the AFA wing, static Navier-Stokes CFD calculations were performed using the EZNSS flow solver that also has aeroelastic capabilities.[10] The flow conditions were chosen to be in the region were limit cycle oscillations often occur, around Mach 0.9 and angles of attack ranging from 0 to 8 degrees. For the calculations, a C-C type mesh was generated about the right side of the AFA wing. The wing was extended to the plane of symmetry to approximately account for the aerodynamic influence of the fuselage. This mesh includes a wing-tip missile and its launcher, but not the under-wing stores. For the sake of compatibility, the linear ZAERO model is based on a similar geometry. A map of the EZNSS surface pressures at AOA=8 degrees is shown in Figure 21.

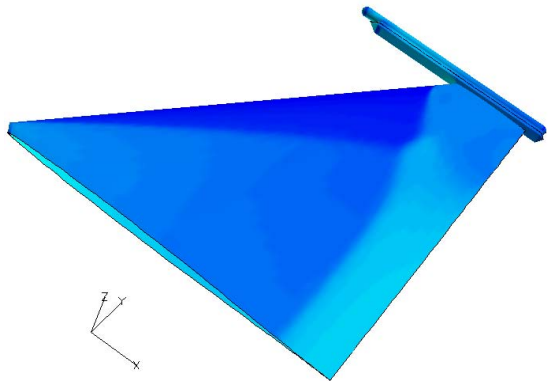

Figure 21: *EZNSS* aerodynamic pressure map for AFA aircraft at Mach 0.9, AOA= 8^{o}

Angle-of-attack effects on C_l (lift coefficient per unit span) and X_{cp} at strips along the span from CFD and from the linear model are shown in Figures 22 and 23, calculated with the pressure distributions at α=0 subtracted. It can be observed that the CFD (EZNSS) C_l distributions are quite linear up to about 6 degrees, where shock-induced separation starts, and that the shocks, visible in Figure 21, move the X_{cp} backwards.

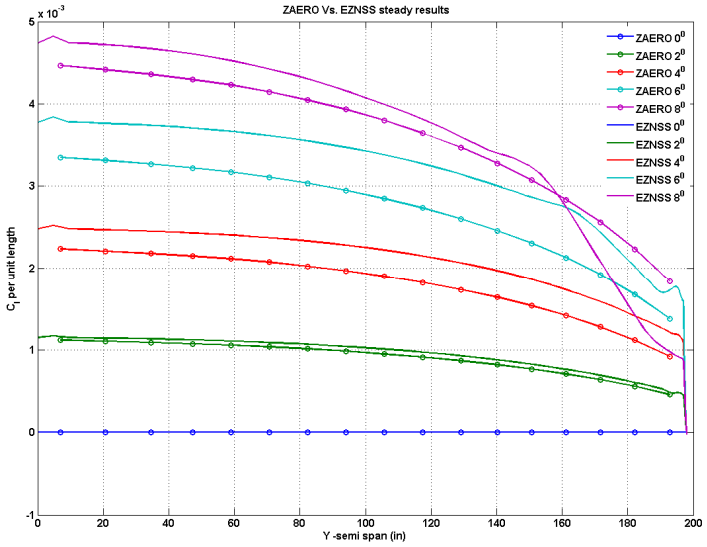

Figure 22: Angle-of-attack effects on C_l along the AFA wing

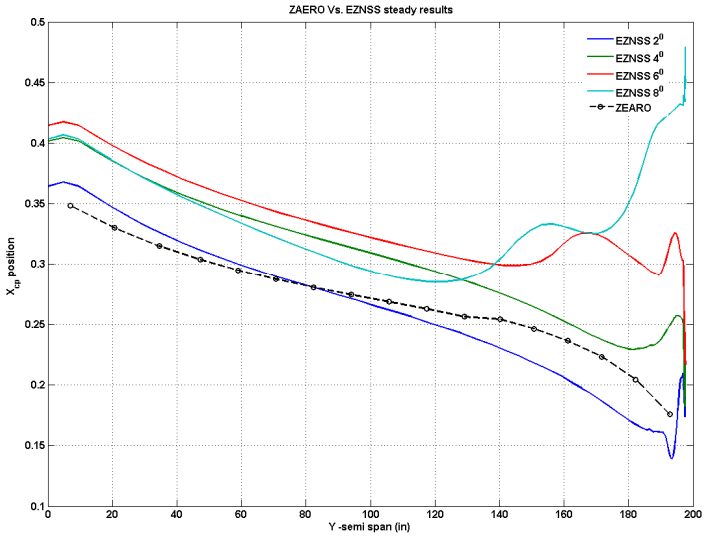

Figure 23: Angle-of-attack effects on X_{cp} along the AFA wing

The C_l distributions along the tip missile, per unit chord, from ZAERO and EZNSS are shown in Figure 24. It can be observed that nonlinear effects move the center of pressure backwards when α increases, and that the rear loads stall above 6 degrees.

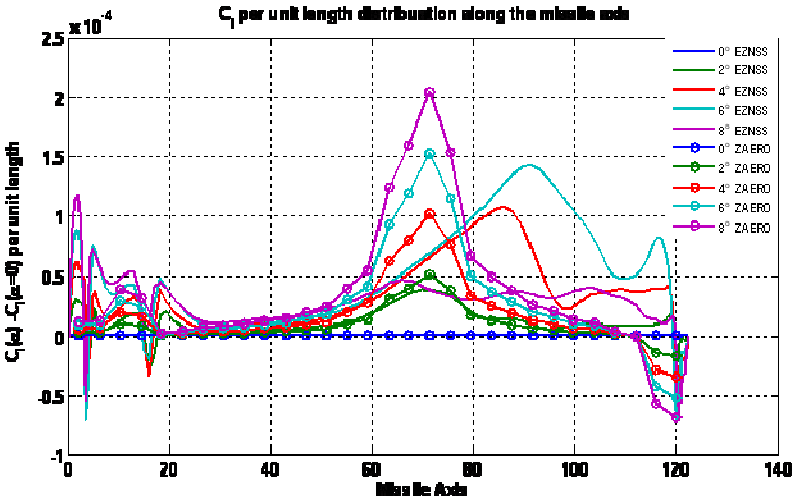

Figure 24: Angle-of-attack effects on C_l along the missile

Linear and nonlinear Lift coefficient vs. AOA at various buttock lines are shown in Figure 25. The nonlinearity at the outer section of the wing above 6 degrees is clear. These plots will serve later in the development of the IOM nonlinear feedback loops.

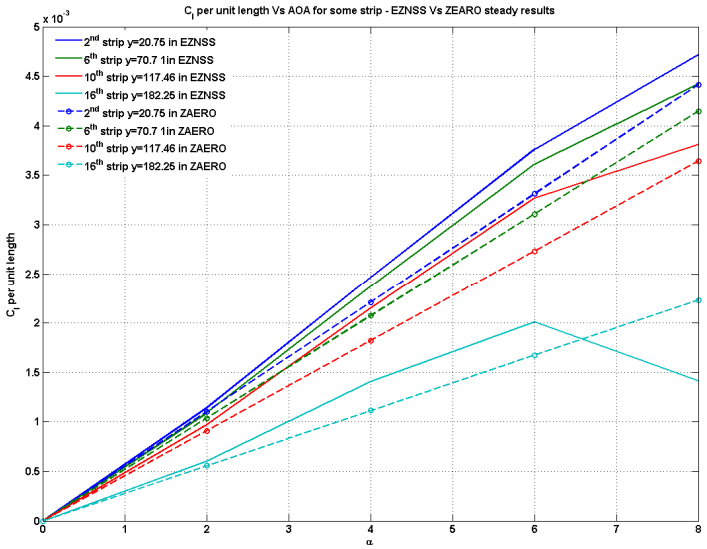

Figure 25: Incremental lift coefficients vs. angle of attach

3.4.3 Linear flutter analysis with corrections

In order to identify the flight conditions at which the Computational Aeroelasticity module of EZNSS is likely to exhibit LCO for the AFA model, the ZAERO linear panel aerodynamic coefficient matrices are corrected for better agreement with the CFD solutions of the previous subsection. The wing was divided into 17 strips as shown in Figure 26. Cl_α and Cm_α (about the local leading edge) of each strip were extracted from CFD by using the differences between α= 0 and 4 degrees. The panels of each strip were assigned with linearly-distributed correction factors tuned to yield the CFD-based Cl_α and Cm_α for each strip. This correction method is based on the assumption that the chordwise bending effects are negligible. The correction factors are shown vs. the panel center X coordinate in Figure 27. It is clear that the factors move the aerodynamic centers backwards, especially at the outer wing. The correction factors along the tip missile, based on CFD pressure distributions at α= 0 and 2 degrees, are also shown in Figure 27

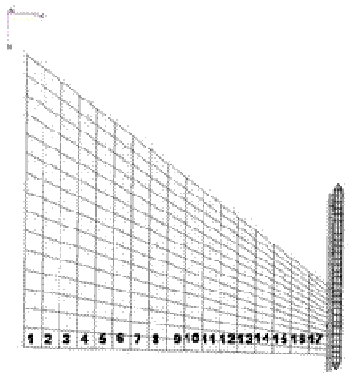

Figure 26: AFA panel model divided into strips.

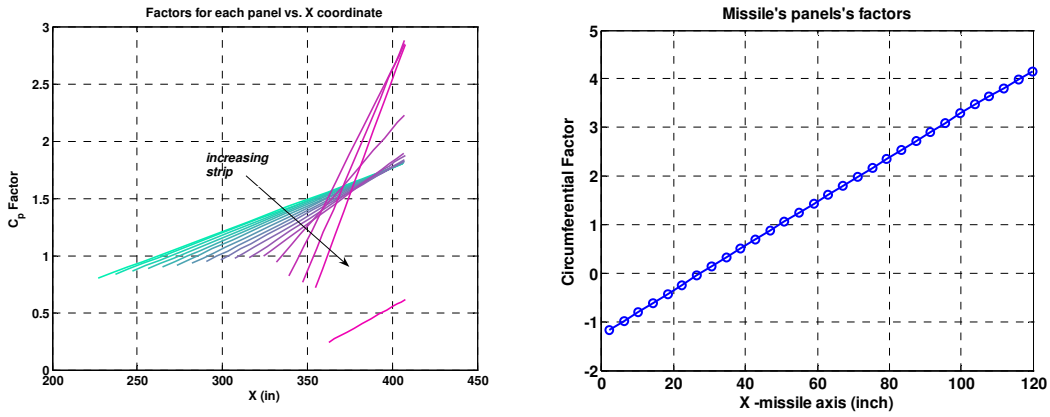

Figure 27: Correction factors at wing strips and at the tip missile.

The correction factors were used to premultiply the unsteady panle coecfficient matrices using the CPFACT option of ZAERO. Figure 28 depicts the resulting variations of frequencies and damping coefficients with the dynamic pressure q. The flutter dynamic pressure and frequency that are obtained using the g-method are q_F= 3126 *psi* and f_F=6.5 *Hz*. It can be noticed that, even though the correction factors generally increase the lift coefficients, the flutter dynamic pressure is increased. This is due to the backwards motion of the aerodynamic centers, which moderated the reduction of the torsion frequency with increasing dynamic pressure, see the solid in Figures 28 and 19. This also causes the flutter mechanism to become even more moderate, which might cause large differences between the CFD-based and the linear flutter dynamic pressures.

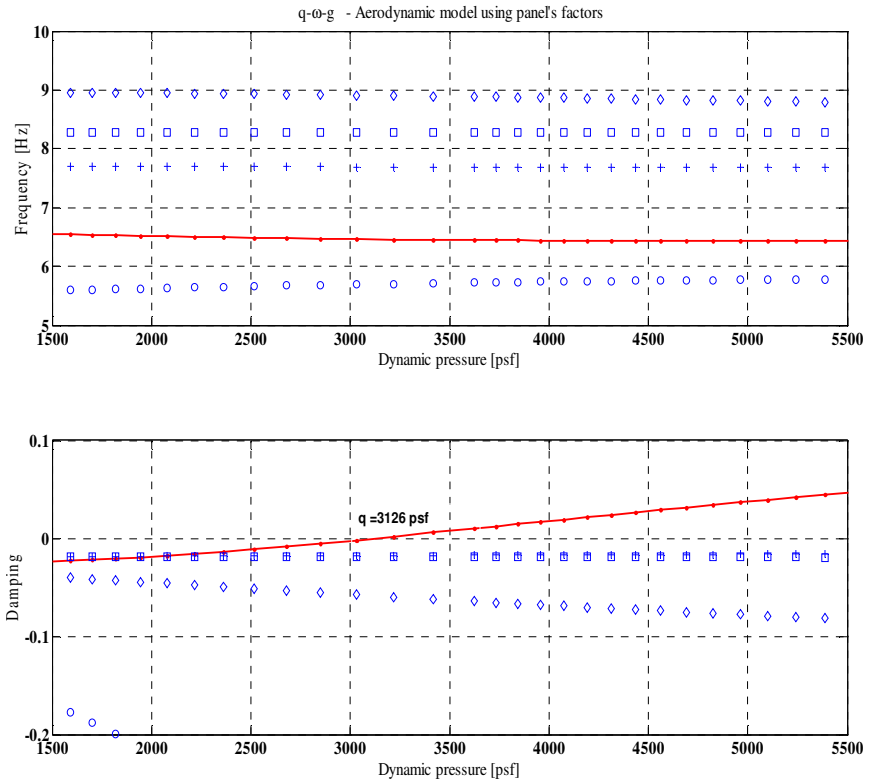

Figure 28: Frequency and damping variations with true air speed, with correction factors

3.4.4 First attempt of LCO calculations with a simple feedback loop

The assumption at this point is that the linear flutter turns into LCO at dynamic pressures higher than q_F due to shock-induced separation at α>6 degrees. The first attempt to define a nonlinear feedback loop that approximates the nonlinear unsteady aerodynamic forces when flutter starts is a simple correction model that adds or subtracts forces and moments according to the steady CFD values discussed above. The correction model is explained with the lift coefficients of the tip missile in Figure 29. The left plot shows the CFD and ZAERO lift values vs. α before any correction. The middle plot demonstrate the way the linear coefficients are corrected as explained in the previous subsection. The right plot is of the nonlinear C_l vs. the would-be one (if the system was linear). A look-up table based on the difference between the two dictates the feedback force that should be added to a selected grid point along the missile. Similar look-up tables are constructed for the lift coefficients of the wing strips and for the moment coefficients. The resulting forces and moments are translated into generalized forces in the AERODYNAMIC CORRECTION box in Figure 7, which are fed back to the plant that is based on the linear state-space model with the linear corrections of the previous subsection. The tables are extended linearly to the coefficient values beyond those of Figure 29.

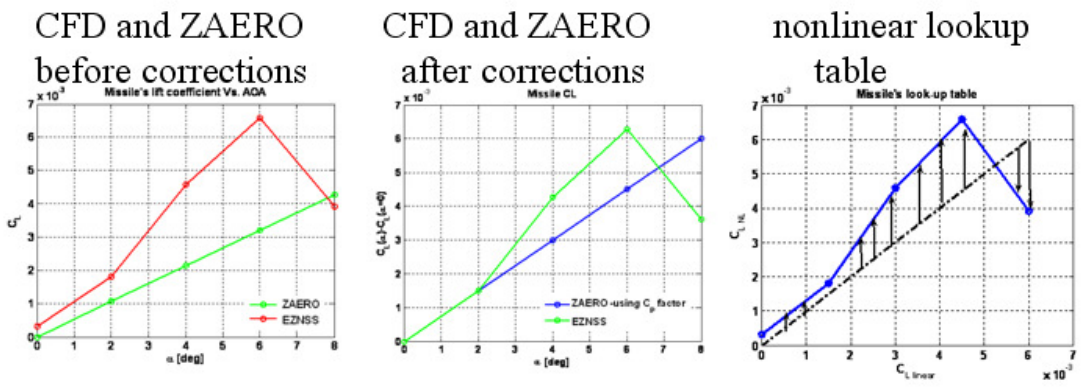

Figure 29: The construction of a lookup table for the basic nonlinear feedback loop

The simulation started with the 1-g α=1.5 degrees at a steady flight at q=3600 *psi*. The incremental pitch angle at Strip 17 is shown in Figure 30, demonstrating an LCO response.

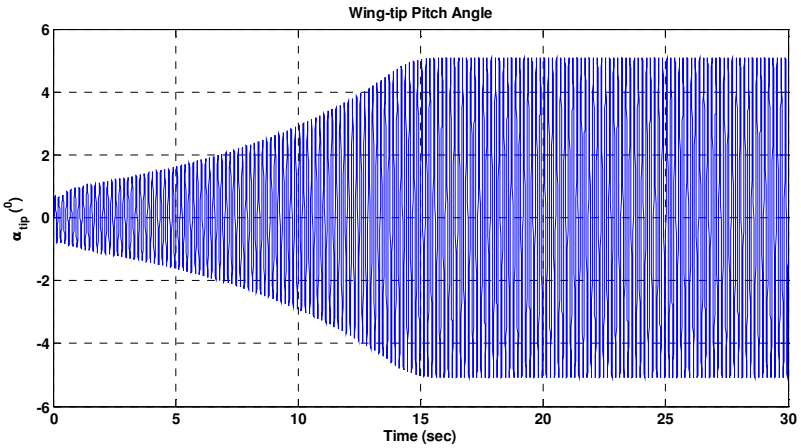

Figure 30: LCO of wing-tip pitch AOA vs. time

3.4.5 Next steps

The next step will be an EZNSS run with a prescribed wing motion defined by the modal response of the IOM LCO simulation of Figure 30. The simulation results will thenbe used to identify an improved feedback model, probably of a higher order, that would better fit the results. With the IOM framework set up, the focus will be on the unsteady characteristics that directly affect the LCO mechanism under investigation.

3.5 Gust response model

The IOM application to gust response with nonlinear aerodynamics in this report is based on the CFD gust response data generated in Ref. 12 for a generic transport aircraft, using the EZNSS code. The structural finite-element model and the CFD surface grid are shown in Figure 31.

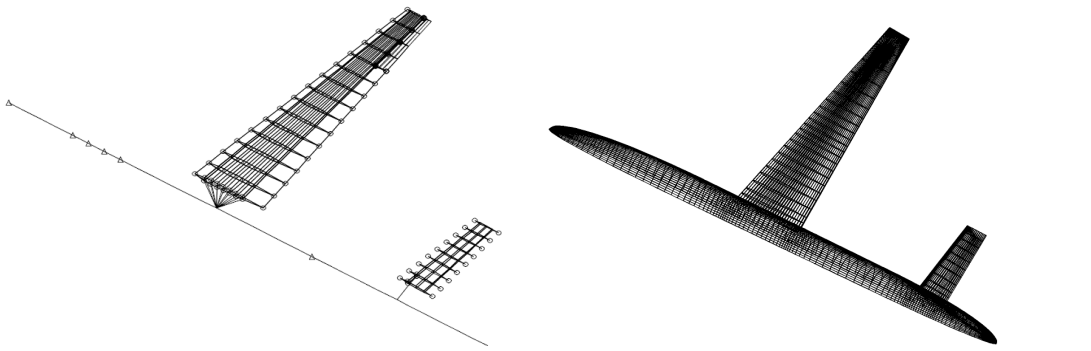

Figure 31: Structural and CFD models of a generic transport aircraft

Steady computations were performed to provide data for establishing the baseline nonlinear feedback model of the IOM process. The resulting aircraft lift coefficients vs. the angle of attack for the rigid and elastic aircraft are shown in Figure 32. The linear curves, based on the nonlinear slopes at low angles of attack, are also shown for comparison. It can be noticed that the differences between the linear and the nonlinear lines for the rigid aircraft are significantly larger than those of the elastic aircraft. This is due to the wash-out effects in the elastic configurations that reduce the wing-tip angles of attack closer to the linear region. It is not clear at this stage what will be the differences in dynamic gust-response cases. Nevertheless, considering the facts that a typical 1-g angle of attack is about 2 degrees, and that a regulation discrete gust may add about 3 degrees to the angle of attack, it can be roughly estimated from the comparisons of Figure 32 that the introduction of nonlinear feedback loops may reduce the peak loads by 5 to 10%. Such reductions are very significant in cases where gust-response loads provide critical structural design loads.

The contributions of the wing to the aircraft lift coefficient (C_L) and to the moment coefficient about CG (C_M), obtained by CFD and with the ZAERO panel model, are shown in Figure 33. While the C_L values of the two models are quite close, the differences in the C_M values indicates that the CFD aerodynamic centers X_α are considerably backwards than

the linear panel-method ones. The pressure distributions over the wing, presented in Figure 34, show that the main reason for the rear X_α values in the CFD results is the rear shock wave.

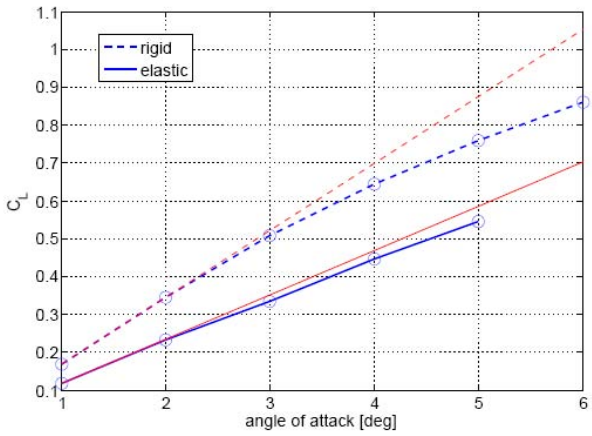

Figure 32: CFD lift coefficient vs. angle of attack, generic transport aircraft

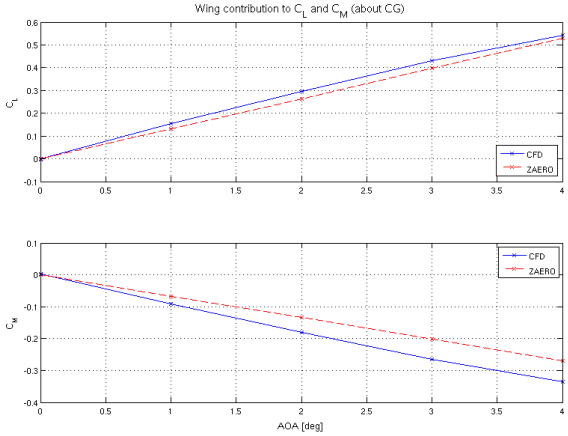

Figure 33: Lift and moment coefficient vs. angle of attack, CFD and ZAERO

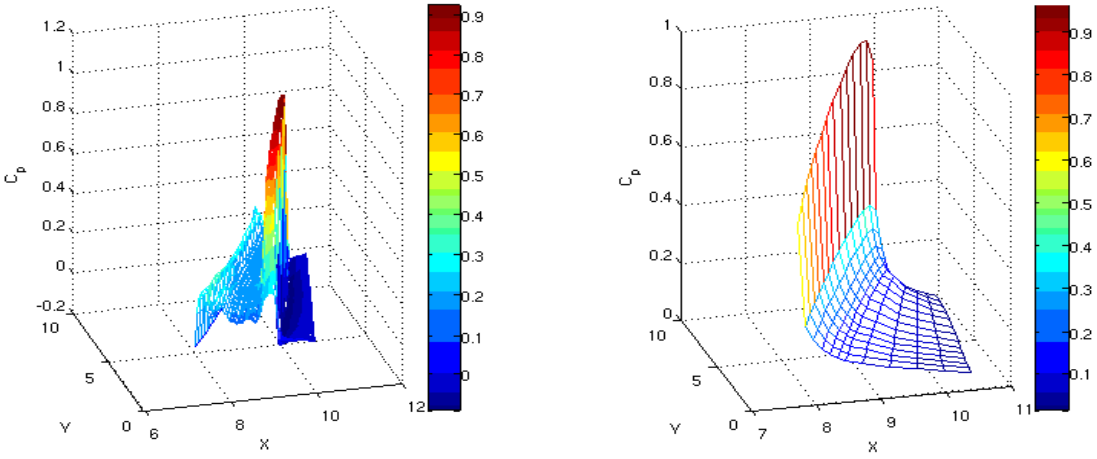

Figure 34: Differential pressure distribution of the wing at α=1°, CFD and ZAERO

The distribution over the wing of lift and moment (w.r.t. the leading edge) coefficients per unit span at various angles of attack in the CFD solution are compared to the linear ones in Figure 35. It is clear that the CFD aerodynamics start to stall at about 3 degrees, especially at the wing-tip region. The X_{cp} comparisons, shown in Figure 36, indicate that X_α moves from the quarter chord in the linear model to about 0.4 chord.

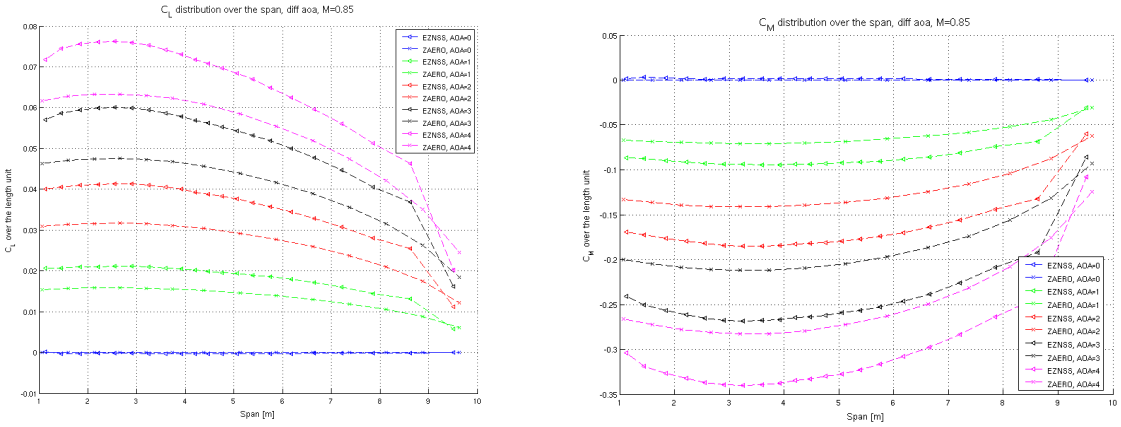

Figure 35: Lift and moment coefficients per unit span over the wing, CFD and ZAERO.

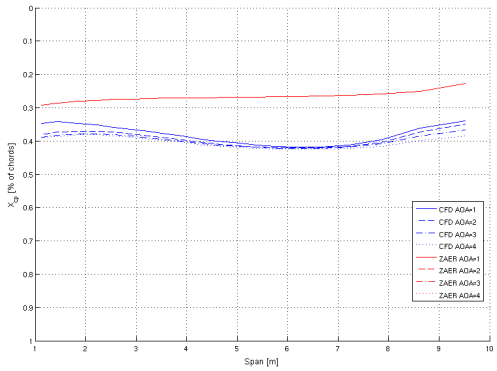

Figure 36: Center-of-pressure distributions over the wing, CFD and ZAERO.

The lift and moment coefficients over the wing at α=1 degree in Figure 35, and those of the tail (not shown), where used to correct the linear ZAERO model. Linearly distributed correction factors were calculated for each panel strip to fit the local C_l and C_m as done in the LCO case of Section 3.4.3. The resulting correction factors over the wing and horizontal tail are shown in Figure 37.

Preliminary results of the aircraft response to gust excitation with the original linear ZAERO model, with the linear model corrected by the factors of Figure 37, and with the

nonlinear IOM based on static corrections based on the C_l and C_m distributions of Figure 35, are shown in Figure 38. The flight conditions are Mach 0.85, h=10kft. The 1-cos vertical gust added at it peak about 4 degrees to the angle of attack. It can be observed that the dynamic response with the corrected linear model is significantly larger than that of the original model. However, when nonlinear feedback corrections are introduced, the loads peaks are reduced by about 10%.

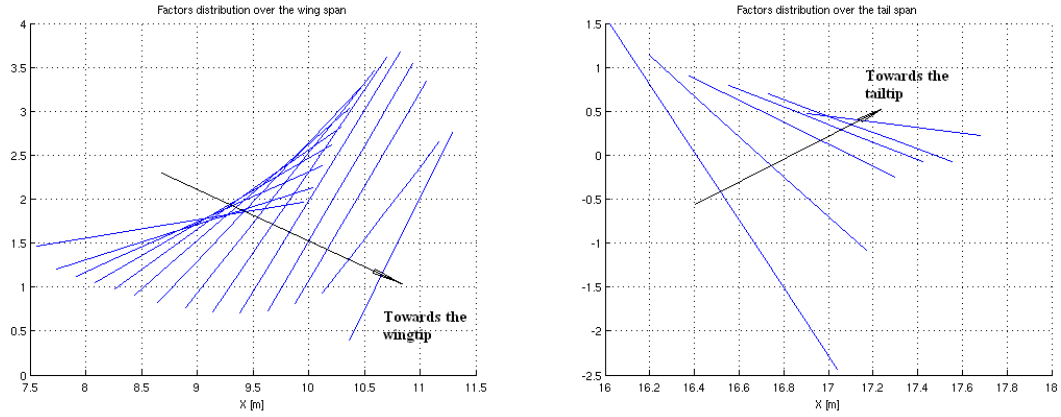

Figure 37: Correction factors at wing and tail strips, GTA model

The next steps will be comparisons of IOM responses to various dynamic responses with the full CFD model in prescribed and in fully aeroelastic cases, and the generation of refined feedback loops to get adequate agreement between the IOM and the CFD models, so massive loads analyses can be performed using IOM.

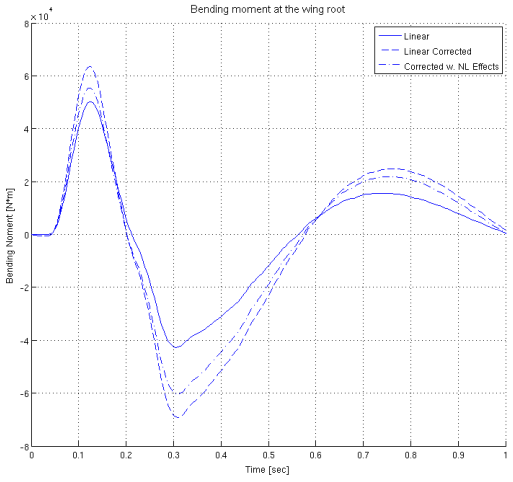

Figure 38: Response to 1-cos discrete gust using linear, corrected linear and IOM models.

4 Conclusions

The IOM framework facilitates efficient and robust expansions of commonly used linear aeroelastic analysis tools to the investigation of a large variety of aereoelastic systems with nonlinear structural, aerodynamic and control elements. The computational tools that were developed recently for aeroelastic response with nonlinear control appear to form a good basis for a general systematic software for IOM applications. Preliminary results in the application of the IOM methodology to aeroelastic problems with nonlinear unsteady aerodynamics indicate that it may enhance the technology of aircraft design by facilitating high-fidelity, yet practical design tools.

Preliminary wing-store LCO models yielded LCO mechanisms similar to those experienced in flight tests, such as the ones reported in Ref. 13. However, the models are not accurate enough for adequately predicting the LCO velocity and amplitude. The refinement of the IOM process with a new aeroelastic CFD model of the AFA wing, based on Navier-stokes solutions, with a detailed wing-tip missile are expected to lead to more valuable LCO prediction tools.

Preliminary results from the application of the IOM approach to discrete gust-response indicate that such applications can be very valuable in aircraft design processes. The enhanced accuracy in massive loads analyses may yield safer and/or more efficient vehicles.

It is recommended to continue the development of the IOM approach in order to substantiate the new framework in which common aeroelastic design tools can be conveniently and efficiently expanded to perform aeroservoelastic simulations with a large variety of nonlinear effects. The tentative plan for the years 2010 to 2012 is:

- Development of a unified IOM software for stability and dynamic response analyses that accommodates aerodynamic, structural and control nonlinearities.
- Facilitate local and distributed nonlinear feedback models.
- Applications with a variety of nonlinear models, from simple local-contact models to full CFD models.
- Systematic identification of nonlinear feedback models based on selected steady and unsteady CFD cases.

- Applications to gust loads with aerodynamic, structural and control nonlinearities
- Accommodation of nonlinear beams in rotary wings.
- Incorporation of free-play modeling in a Stick-to-Stress simulator.

5 References

1. Karpel, M., Shousterman, A., Maderuelo, C., Anguita, L., Climent, H., "Dynamic Gust Response with Nonlinear Control Using Frequency Domain Models", Paper No. 2009-107, Proceedings of the International Forum on Aeroelasticity and Structural Dynamics, Seattle, WA, June 2009.
2. Karpel, M., Moulin, B., Presente, E., Anguita, L., Maderuelo, C. and Climent, H. "Dynamic Response To Gust Excitation With Nonlinear Control Systems", Paper IF-072, Proceedings of the International Forum on Aeroelasticity and Structural Dynamics, Stockholm, Sweden, June 2007.
3. Gold, P. and Karpel, M., "Reduced-Size Aeroservoelastic Modeling and Limit-Cycle-Oscillation Simulations with Structurally non-Linear Actuators," Journal of Aircraft, Vol.45, No. 2, 2008, pp. 471-477.
4. Levin, D. and Karpel, M., "Limit Cycle Oscillations of Plate-Type Fins Using Increased-Order Models", AIAA Paper 2010-2634, to be presented at the 51st AIAA/ASME/ ASCE/AHS/ASC Structures, Structural Dynamics, and Materials Conference, Orlando, FA, April 2010.
5. Karpel, M., Hollander, Y., Gur, I., E. and Levy, Y., "Increased-Order Models for the Prediction of Aeroelastic Limit Cycle Oscillations", in 49th AIAA/ASME/ ASCE/AHS/ASC Structures, Structural Dynamics, and Materials Conference, Chicago, IL, April 2008.
6. Karpel, M., "Time-Domain Aeroservoelastic Modeling Using Weighted Unsteady Aerodynamic Forces," Journal of Guidance, Control, and Dynamics, Vol. 13, No. 1, 1990. pp. 30-37.
7. P. J. Attar, E. H. Dowell, J. R. White, *Modeling Delta Wing Limit-Cycle Oscillations Using a High-Fidelity Structural Model*, Journal of Aircraft Vol. 42, No. 5, September-October 2005, pp. 1209-1217.
8. Gordnier, R. E., "Computation of Limit-Cycle Oscillations of a Delta Wing," Journal of Aircraft, Vol. 40, No. 6, 2003.

9. Attar, P. J. and Gordnier, R. E., “Aeroelastic Prediction of the Limit Cycle Oscillations of a Cropped Delta Wing,” Journal of Fluids and Structures, No. 6, 2006, pp. 45-58.
10. Raveh, D.E., Levy, Y., and Karpel, M., "Efficient Aeroelastic Analysis Using Computational Unsteady Aerodynamics," Journal of Aircraft, Vol. 38, No. 3, 2001, pp. 547-556.
11. Raveh, D. E., “CFD-Based Models of Aerodynamic Gust Response” Journal of Aircraft. Vol. 44, No. 3, May-June 2007, pp. 888-897.
12. Raveh, D.E. “CFD-Based Gust Response Analysis of Free Elastic Aircraft” in 50th AIAA/ASME/ASCE/AHS/ASC Structures, Structural Dynamics, and Materials Conference, Palm Springs, CA, May 2009.
13. Denegri, Jr., C.M., “Limit-Cycle Oscillation Flight Test Results of a Fighter with External Stores,” Journal of Aircraft, Vol. 37, No. 5, pp. 761-769, 2000.